Materials Horizons

ROYAL SOCIETY OF CHEMISTRY

COMMUNICATION

View Article Online
View Journal | View Issue

Cite this: *Mater. Horiz.*, 2023, 10, 607

Received 2nd September 2022,
Accepted 30th November 2022

DOI: 10.1039/d2mh01100j

rsc.li/materials-horizons

Backbone coplanarity manipulation *via* hydrogen bonding to boost the n-type performance of polymeric mixed conductors operating in aqueous electrolyte†

Junxin Chen,[a] Shengyu Cong,*[a] Lewen Wang,[a] Yazhou Wang,[a] Liuyuan Lan,[a] Chaoyue Chen,[a] Yecheng Zhou,[a] Zhengke Li,[a] Iain McCulloch[b] and Wan Yue*[a]

The development of high-performance n-type semiconducting polymers remains a significant challenge. Reported here is the construction of a coplanar backbone *via* intramolecular hydrogen bonds to dramatically enhance the performance of n-type polymeric mixed conductors operating in aqueous electrolyte. Specifically, glycolated naphthalene tetracarboxylicdiimide (gNDI) couples with vinylene and thiophene to give gNDI-V and gNDI-T, respectively. The hydrogen bonding functionalities are fused to the backbone to ensure a more coplanar backbone and much tighter π–π stacking of gNDI-V than gNDI-T, which is evidenced by density functional theory simulations and grazing-incidence wide-angle X-ray scattering. Importantly, these copolymers are fabricated as the active layer of the aqueous-based electrochromic devices and organic electrochemical transistors (OECTs). gNDI-V exhibits a larger electrochromic contrast (ΔT = 30%) and a higher coloration efficiency (1988 $cm^2\ C^{-1}$) than gNDI-T owing to its more efficient ionic–electronic coupling. Moreover, gNDI-V gives the highest electron mobility (0.014 $cm^2\ V^{-1}\ s^{-1}$) and μC^* (2.31 $F V^{-1}\ cm^{-1}\ s^{-1}$) reported to date for NDI-based copolymers in OECTs, attributed to the improved thin-film crystallinity and molecular packing promoted by hydrogen bonds. Overall, this work marks a remarkable advance in the n-type polymeric mixed conductors and the hydrogen bond functionalization strategy opens up an avenue to access desirable performance metrics for aqueous-based electrochemical devices.

New concepts

In recent years, considerable efforts have been put into designing polymeric mixed ionic–electronic conductors (PMIECs), as they are key to advancing a host of technological developments for electrochemical devices. However, the development of high-performance n-type PMIECs remains a significant challenge. While extensive research has gone into introducing novel building blocks or diverse hydrophilic pendant chains (e.g., butylene glycol) to maximize the performance of n-type PMIECs operating in aqueous electrolyte, little work has thus far been conducted on tailoring the molecular packing and electronic properties through conformational control using intramolecular hydrogen bonds. Herein, we report the very first high performance n-type PMIECs developed by backbone coplanarity manipulation *via* hydrogen bonds, which were fabricated as aqueous-based electrochromic devices and organic electrochemical transistors. In particular, the more coplanar backbone conformation driven by intermolecular hydrogen bonds results in a much higher device performance in both aqueous-based devices. Importantly, the first demonstration of backbone coplanarity control *via* hydrogen bonding promises to expand our understanding of the effect of backbone conformation on ionic–electronic coupling and mixed conduction in aqueous media. We envisage our systematic work will inspire researchers from diverse backgrounds to design future n-type PMIECs to promote their developments for application in next-generation bioelectronics, optoelectronics and batteries.

1. Introduction

Organic mixed ionic–electronic conductors (OMIECs) are often conjugated polymers (CPs), and can simultaneously transport ionic and electronic species.[1,2] CPs are a perfect candidate for mixed conduction: a conjugated backbone supports the charge transport and the ionic transport is allowed through the bulk.[3,4] More importantly, the desired properties can be facilely introduced to CPs *via* chemical modifications.[5,6] Based on these advantages, there has been growing interest in developing CPs which can be reversibly doped and de-doped with aqueous electrolyte.[7,8] As reported, an aqueous-based electrolyte possesses high ionic conductivity, incombustibility and non-toxicity, which makes it a promising alternative to an

[a] *Guangzhou Key Laboratory of Flexible Electronic Materials and Wearable Devices, Key Laboratory for Polymeric Composite and Functional Materials of Ministry of Education, School of Materials Science and Engineering, State Key Laboratory of Optoelectronic Materials and Technologies, Sun Yat-sen University, Guangzhou 510275, P. R. China. E-mail: congshy@mail.sysu.edu.cn, yuew5@mail.sysu.edu.cn*

[b] *Department of Chemistry, Chemistry Research Laboratory, University of Oxford, Oxford OX1 3TA, UK*

† Electronic supplementary information (ESI) available. See DOI: https://doi.org/10.1039/d2mh01100j

organic electrolyte.[9,10] Therefore, CPs operating in aqueous electrolyte possess much potential to fabricate as active materials to develop non-toxic and environment-friendly electrochemical devices, such as light-emitting electrochemical cells (LEEC),[11] organic electrochemical transistors (OECTs)[12] and electrochromic devices (ECDs).[13]

However, most CPs are hydrophobic which results from their hydrophobic alkyl side chains and conjugated backbones.[14,15] Introducing hydrophilic oligo (ethylene glycol) (OEG) as side chains is a prevailing method to promote the ionic conductivity of CPs in aqueous electrolyte and provide sufficient solubility in organic solvents for solution processing.[16–18] Generally, the CPs as OMIECs can be classified as p-type and n-type.[19,20] Compared to the well-developed p-type OMIECs, the development of n-type OMIECs is relatively slow.[21,22] Whereas the n-type OMIECs are highly essential as electron-transporting materials for realizing p–n-junction-based wearable, flexible or printable electrochemical devices,[23] such as low-power OECT-based complementary circuits for bioelectronic applications,[24] thus it is indispensable and imperative to develop high-performance n-type polymeric mixed conductors. However, compared with p-type OMIECs, the n-type OMIECs more easily suffer from the issue of "nonplanar backbones".[25,26] This is attributed to the electron-withdrawing groups (such as C═O or C≡N), which enable the n-type charge transport properties, are often bulky and likely induce a steric hindrance on their adjacent subunits.[27] Furthermore, such steric hindrance may potentially result in a highly twisted backbone, which would shorten the coherent conjugation length and inhibit the interchain carrier transport, thus limiting the transport of charge carriers with respect of electrochemical application.[28,29]

One promising approach to address the aforementioned "nonplanar backbone" issue of the n-type OMIECs is the employment of noncovalent bonds to construct coplanar conformation.[30,31] Among various types of noncovalent interactions, the hydrogen bond works as an ideal interaction owing to its tunable strength, directional nature and synthetic versatility which allow for precise control of backbone conformation.[32–34] The noncovalent conformational lock effect driven by hydrogen bonds can be viewed as high energy barriers which prevent the low energy coplanar conformer from torsional rotation, contributed by the formation of noncovalent interactions.[28] Much research has reported intriguing properties which were induced by the coplanar conformation, such as anisotropic molecular aggregation and solvent resistance.[35] Moreover, a coplanar backbone is expected to possess effective coherent conjugation along the backbone and provide faster intramolecular charge transport.[35,36] Additionally, coplanarity conformation favors small reorganization energy through charge transport and close intermolecular packing, which would result in strong intermolecular electronic coupling and long exciton diffusion length.[36] Despite the potential of the hydrogen bond functionalization, especially rare are works reporting the performance enhancement of n-type polymeric mixed conductors operating in aqueous media through backbone coplanarity manipulation by hydrogen bonds.

Naphthalenediimide (NDI) has been well utilized as a robust building block for n-type OMIECs and NDI groups have high thermal and oxidative stability.[37,38] The strongly electron-deficient aromatic unit with two electron-withdrawing imide groups gives low-lying LUMO energy levels, which makes NDI-based CPs excellent electron-transporting semiconductors.[39,40] Besides, NDI-based copolymers usually exhibit good long-term operational stability in water, which is critical for practical aqueous-based applications.[41,42] Additionally, much potential was found in NDI-based copolymers as electrochromic displays and energy storage devices, which can be used as a platform for varied aqueous-based electrochemical devices.[16] However, the carbonyl groups in the NDI core often cause a strong steric hindrance with the adjacent units and a twisted backbone conformation,[43,44] consequently resulting in localized polaron and limited carrier transport.[45,46] For instance, our previous work investigated glycolated NDI coupling with bithiophene to give **gNDI-BT**, which was fabricated as a channel material in OECTs.[16] It was found that **gNDI-BT** exhibited a highly twisted backbone and relatively large dihedral angles (θ) up to 44°, which was evidenced by density functional theory (DFT) calculations. Furthermore, DFT computations revealed that the twists mainly occurred between the NDI core and the adjacent thienyl groups. As a consequence, less ordered molecular packing was found and **gNDI-BT** presented a low electron mobility of 5.69×10^{-4} cm^2 V^{-1} s^{-1} in OECTs.

Inspired by the potential of hydrogen bond functionalization to construct a coplanar backbone conformation, the molecular structure–device property correlation for n-type OMIECs operating in aqueous media has been systematically investigated. NDI was employed as an acceptor unit in this work, coupling with vinylene and thiophene to give **gNDI-V** and **gNDI-T**, respectively. DFT simulations support that the **gNDI-V** displays a coplanar backbone conformation owing to intramolecular hydrogen bonds, while **gNDI-T** exhibits a highly twisted backbone without an intermolecular hydrogen bond. Furthermore, **gNDI-V** exhibited much shorter π–π stacking (3.59 Å) than **gNDI-T** (3.97 Å). The relationship between polymeric structure and device properties has been established by systemically comparing the NDI copolymers' optical and electronic properties, electrochemical charging behavior and spectroelectrochemical properties, molecular packing, as well as a range of electrochemical device performances (ECDs and OECTs). It was observed that **gNDI-V** gave superior device performances than **gNDI-T**, including greater electrochromic contrast and composite coloration efficiency as ECDs. Compared to **gNDI-T**, the OECTs based on **gNDI-V** exhibit an impressive electron mobility of 0.014 cm^2 V^{-1} s^{-1} and an excellent μC^* value of 2.31 F V^{-1} cm^{-1} s^{-1}, which are both the highest values reported to date for NDI-based OMIECs. Therefore, the proposed hydrogen bond functionalization will inspire future molecular design and varied n-type copolymers can be optimized by this design principle to access desirable performance metrics in aqueous-based electrochemical devices.

2. Results and discussion

2.1 NDI-based copolymers synthesis

Two NDI-based copolymers synthesized in this work are illustrated in Scheme 1. The synthetic procedures for the monomers and copolymers are described in Schemes S1 and S2 (ESI†). The six OEG repeating units were utilized to provide the NDI-based copolymers with essential ionic conductivity in aqueous media and high solubility in organic solvents for solution processing. The **gNDI** for the polymerization was synthesized according to our previous report.[16] The *trans*-1, 2-bis(tributylstannyl)ethene and 2,5-bis(trimethylstannyl)thiophene were both commercially available. Under typical Stille polymerization conditions, the **gNDI** monomer was polymerized with the two forementioned monomers to give **gNDI-T** and **gNDI-V** in high yields. Specifically, **gNDI-T** and **gNDI-V** are both insoluble in aqueous media, which allows characterization of their device properties in aqueous electrolyte. In addition, the two copolymers both exhibited good solution processability with adequate solubility (equal to or above 20 mg mL^{-1}) in common organic solvents, such as chloroform and dichloromethane. The molecular weights of **gNDI-T** and **gNDI-V** were evaluated by matrix-assisted laser desorption/ionization time-of-flight (MALDI-TOF) mass spectrometry, exhibiting the maximum molecular weights between 16.3 and 17.2 kDa, corresponding to the repeating units of 19 (Fig. S7, ESI†). The number-average molecular weights (M_n) for the two copolymers were also determined by gel permeation chromatography (GPC) and the M_n was in the range between 11.0 and 15.9 kDa (Fig. S8, ESI†), which was in accordance with the MALDI-TOF data. Their thermal properties were characterized by the thermogravimetric analysis (TGA), showing good thermal stabilities with a decomposition temperature over 290 °C for both copolymers (Fig. S9, ESI†).

2.2 Optical and electronic properties

The optical properties of NDI-based copolymers were measured by UV-vis-NIR absorption measurement and the corresponding data are summarized in Table 1. As illustrated in Fig. 1a, all the absorption spectra exhibited similar absorption profiles with dual-band absorption, an absorption band in the high energy range (309–445 nm) attributed to the π–π* transition and a low energy (422–746 nm) band which originated from the intramolecular charge transfer (ICT).[47] In the solution, an absorption maximum (λ_{max}) of low energy band located at 520 nm and 544 nm was recorded for **gNDI-V** and **gNDI-T**, respectively. By monitoring the film absorption spectra, the λ_{max} of **gNDI-V** and **gNDI-T** presented an apparent red-shift compared with their solution absorption, suggesting improved molecular packing in solid states.[48] Note that the absorption maximum (λ_{max}) shifts significantly from 532 nm for **gNDI-V** to 623 nm for **gNDI-T**. The red shift was likely due to the stronger electron-donating ability of the thiophene unit than that of the vinylene unit, which is evidenced by the later cyclic voltammetry (CV) measurements and density functional theory (DFT) simulations. The optical bandgaps (E_g^{opt}) were obtained from the film absorption onsets, and the values are 1.73 eV for **gNDI-T** and 2.01 eV for **gNDI-V**. The lower bandgap of **gNDI-T** is attributed to the relatively stronger ICT character between the NDI and the thiophene unit.[49]

To evaluate the electrochemical properties of the NDI-based copolymers, CV measurements were performed in acetonitrile with 0.1 M tetrabutylammonium hexafluorophosphate (n-Bu_4NPF_6) using Ag/AgCl as a reference electrode. As illustrated in Fig. 1b, the reduction onset potential in acetonitrile of **gNDI-T** and **gNDI-V** was −0.21 V and −0.02 V, respectively. Then, the corresponding lowest unoccupied molecular orbital

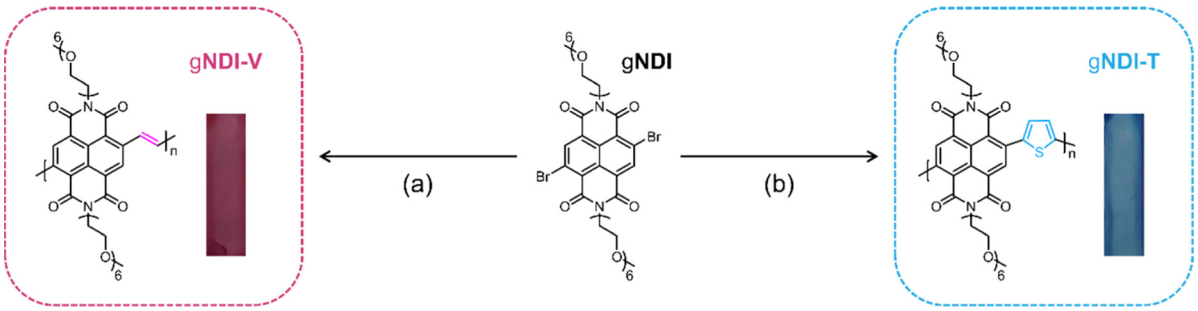

Scheme 1 NDI-based copolymers synthesized in this work (the color represents the resulting polymer film color). Reaction conditions: (a) *trans*-1, 2-bis(tributylstannyl)ethene, $Pd_2(dba)_3$, P(*o*-tol)$_3$, toluene, 110 °C, 24 h; (b) 2,5-bis(trimethylstannyl)thiophene, $Pd_2(dba)_3$, P(*o*-tol)$_3$, toluene, 110 °C, 24 h.

Table 1 Optical and electrochemical properties of the NDI-based copolymers

Polymer	$\lambda_{max,solution}$[a] (nm)	$\lambda_{max,film}$[b] (nm)	E_{LUMO}[c] (eV)	E_{HOMO}[d] (eV)	E_g^{opt}[e] (eV)	$E_{red,aq}$[f] (V)
gNDI-V	328, 520	329, 532	−4.40	−6.43	2.01	0.06
gNDI-T	325, 544	348, 623	−4.21	−5.94	1.73	0.13

[a] Solution. [b] Thin film. [c] E_{LUMO} was calculated from the equation $E_{LUMO} = -[4.8 + E_{red(onset)} - E_{FOC}]$ V, where the E_{FOC} is +0.38 V with Fc/Fc^+ as an external standard. [d] $E_{HOMO} = E_{LUMO} - E_g^{opt}$. [e] Obtained from the absorption onset of thin film ($E_g^{opt} = 1240/\lambda_{onset}$). [f] Estimated from the onset of the first reduction peak in 0.1 M KCl at a scan rate of 100 mV s^{-1}.

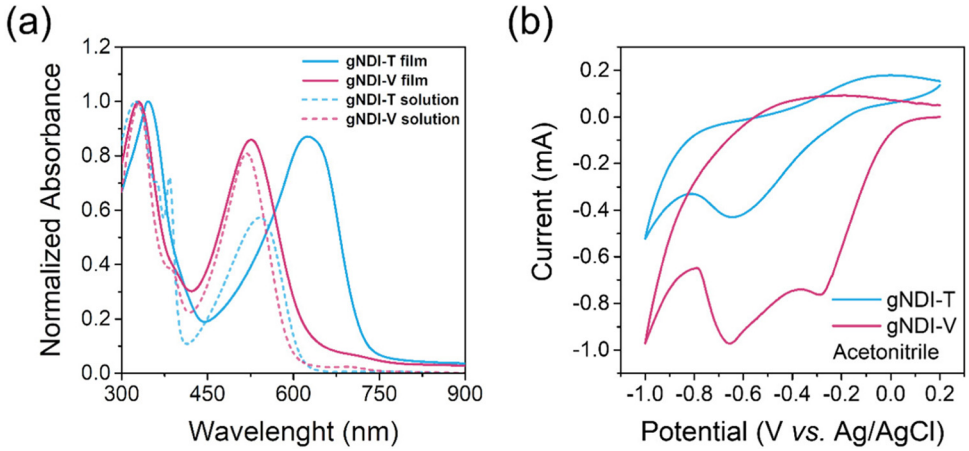

Fig. 1 (a) UV-vis-NIR absorption spectra of NDI-based copolymers. (b) Cyclic voltammetry of the polymer films in 0.1 M tetrabutylammonium hexafluorophosphate (n-Bu_4NPF_6) acetonitrile solution at a scan rate of 100 mV s^{-1}.

(LUMO) energy levels (E_{LUMO}) were calculated as −4.21 eV for **gNDI-T** and −4.40 eV for **gNDI-V**. Notably, **gNDI-T** and **gNDI-V** both present low-lying LUMO (< −4.02 eV), which has favorable energetics to avoid the electron trapping by water and oxygen.[50,51] The highest occupied molecular orbital (HOMO) energy level (E_{HOMO}) was obtained by using E_{LUMO} subtracting an optical band gap (E_g^{opt}) to give the value of −5.94 eV for **gNDI-T** and −6.43 eV for **gNDI-V**. According to the literature, for NDI-based copolymers, the E_{LUMO} is dominantly influenced by the NDI contribution while the E_{HOMO} is sensitive to the relative electron-donating strength of donor units.[52,53] A significant increase in the E_{HOMO} changing from vinylene to thiophene is observed, which indicates the destabilization of E_{HOMO} with increasing electron donating strength.[54]

2.3 Coplanar backbone conformation analysis

To gain an insight into the backbone geometries and electronic structures, DFT by Gaussian 09 with the level of B3LYP/6-31G(d) was carried out. The OEG side chains were simplified as the methyl group. The optimized backbone geometry and frontier molecular orbitals of both trimers are presented in Fig. 2a and c. First, the **gNDI-V** trimer presents a more coplanar backbone geometry than the **gNDI-T** trimer from the side view. Besides, for the **gNDI-V** trimer, the distance between the O atom

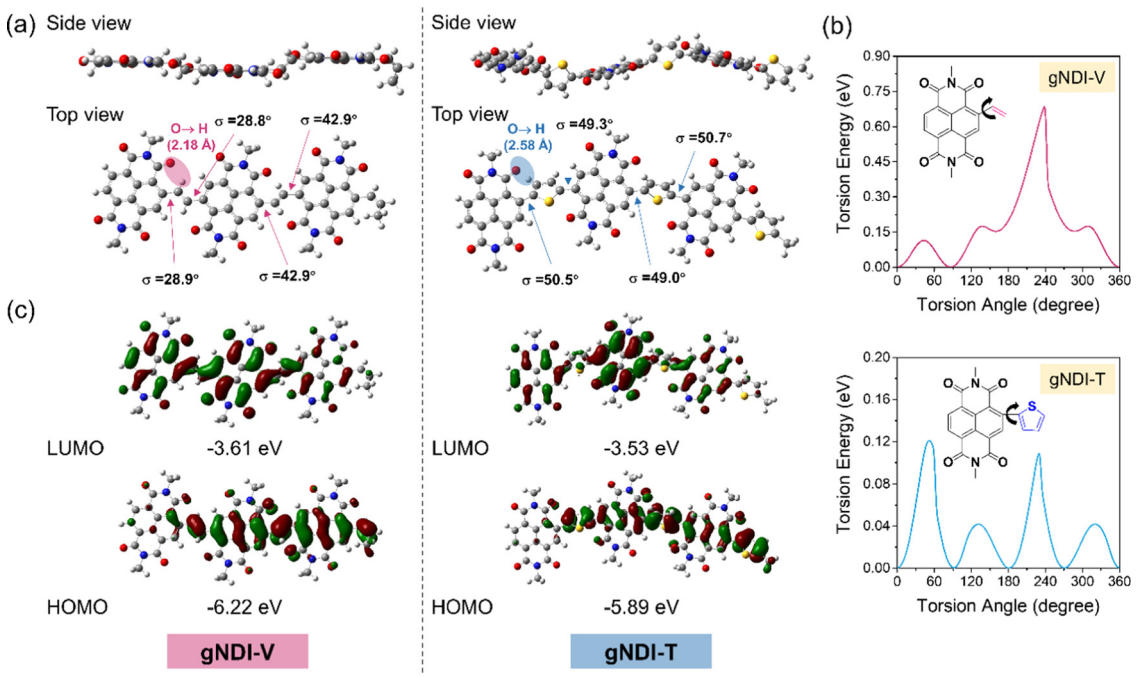

Fig. 2 (a) The optimized molecular geometries and dihedral angles of NDI-based trimers. The red and blue circles present the distance between the O atom from NDI and the H atom from the vinylene or thiophene unit. (b) Torsion energy profiles of the **gNDI-V** and **gNDI-T** trimers. (c) Energy levels and visualization of LUMOs and HOMOs of NDI-based trimers.

(the carbonyl of NDI) and the H atom (vinylene) is 2.18 Å, much shorter than the sum of the O and H van der Waals radii of 2.50 Å,[55,56] which indicates the presence of the O···H hydrogen bond, contributing to the reduction in the conformational disorder by locking the rotating single bond. However, the **gNDI-T** trimer indicates the distance between the O atom (the carbonyl of NDI) and H atom (thiophene) is 2.58 Å, larger than the sum of the O and H van der Waals radii, suggesting the absence of O···H noncovalent interactions. As a consequence, the **gNDI-V** trimer displays a coplanar backbone conformation with a dihedral angle around 35° between the NDI and the adjacent vinylene, while a more twisted backbone with a dihedral angle around 50° between the NDI and thiophene is found for the **gNDI-T** trimer. In addition, Fig. 2b illustrates the torsion energy for both trimers and it is found that the **gNDI-V** trimer gives a larger torsion energy barrier (~0.69 eV) than the **gNDI-T** trimer (~0.12 eV), enabling the **gNDI-V** trimer to have a more rigid backbone, since the hydrogen bond works as a non-bonding conformational lock.[43] Furthermore, the coplanar backbone would potentially prolong the coherent conjugation length and enhance interchain charge carrier transport.[57] Besides, the visualization of LUMOs and HOMOs is shown in Fig. 2c. The two trimers revealed localized electronic structures: the donor units contribute mainly to the HOMOs while the LUMOs are highly localized on electron deficient NDI. The calculated E_{LUMO}/E_{HOMO} of **gNDI-V** (−3.61/−6.22 eV) was deeper than that of **gNDI-T** (−3.53/−5.89 eV), which was consistent with the CV measurement results. Similarly, the increased E_{HOMO} in **gNDI-T** calculated from DFT simulations indicate the stronger electron-donating ability of the thiophene unit. Moreover, the DFT computation results reveal that the hydrogen bond functionalities finely modulate the n-type conjugated backbone conformation.

2.4 Microstructure study

To further study the effect of the hydrogen bond on polymer packing orientation, the NDI-based copolymer thin-film microstructures were analyzed by grazing-incidence wide-angle X-ray scattering (GIWAXS). The GIWAXS characteristics of both copolymers are shown in Fig. 3 and the corresponding parameters are summarized in Table S1 (ESI†). The **gNDI-V** displayed a strong (010) scattering peak in the out-of-plane direction while the **gNDI-T** concurrently showed lamellar scattering (100) peaks in the out-of-plane direction and a π–π stacking (010) peak in both the out-of-plane and in-plane direction, suggesting that the **gNDI-V** presented a predominant face-on orientation and the **gNDI-T** exhibited a mixed face-on/edge-on orientation. Fig. 3c shows a comparison of the π–π stacking distance and paracrystalline disorder in π–π stacking direction for both copolymers. It is found that the π–π stacking distance sharply decreased from 3.97 Å for **gNDI-T** to 3.59 Å for **gNDI-V.** The closer intermolecular packing in the solid state of **gNDI-V** likely results from its coplanar backbone conformation.[55] Additionally, the paracrystalline disorder parameter, strongly correlating with electrical conductivity, was calculated according to eqn (1)[58]

$$g = \sqrt{\frac{\mathrm{FWHM}}{2\pi q}} \tag{1}$$

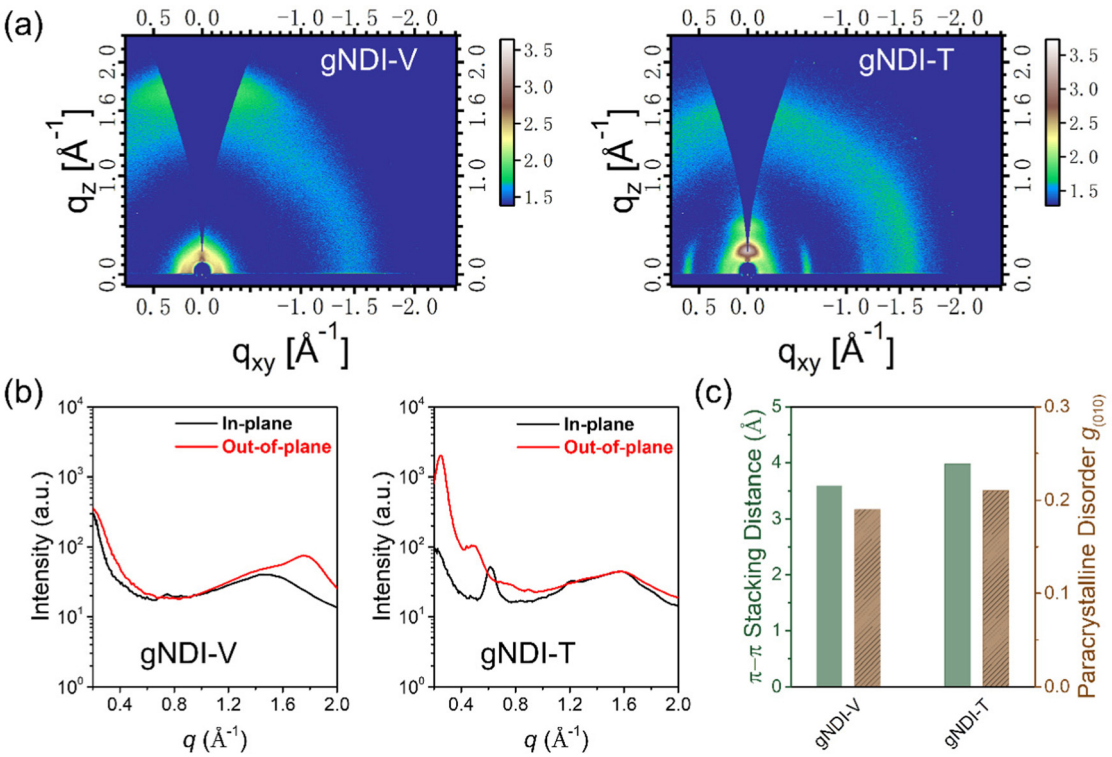

Fig. 3 (a and b) 2D GIWAXS patterns of thin films of gNDI-V and gNDI-T, and corresponding line-cut profiles along the in-plane and out-of-plane directions; (c) π–π stacking distance and paracrystalline disorder in the π–π stacking direction for both copolymers.

where the FWHM presents a diffraction peak full width at half-maximum, and q is the diffraction peak position. The paracrystalline disorder of π-stacking direction $g_{(010)}$ calculated from this equation decreased from 0.21 for **gNDI-T** to 0.19 for **gNDI-V**, and a decrease in $g_{(010)}$ indicates the hopping transfer integral and conductivity enhancement.[59] Together with the much shorter π–π spacing and lower paracrystalline disorder in **gNDI-V**, we believe the manipulation of backbone coplanarity *via* the introduction of hydrogen bonding can improve the thin-film crystallinity and bring more favorable molecular packing to facilitate charge transport. Moreover, to analyze the microstructure features of polymer films upon electrochemical doping, we collected GIWAXS of the films in their reduced condition (see Fig. S10 and Table S2, ESI†). Compared with the pristine state, there were no obvious film microstructure changes in the reduced state for both NDI-based copolymers, which indicates a good operation stability in aqueous electrolytes.[60]

2.5 Electrochemical charging with aqueous electrolyte

To investigate the electrochemical redox behavior, CV measurement of polymer thin films in 0.1 M KCl aqueous solution at a scan rate of 100 mV s^{-1} was conducted (see Fig. 4). The reduction onset potential of the copolymers in aqueous media was 0.13 V for **gNDI-T** and 0.06 V for **gNDI-V** (Fig. S11, ESI†). However, the reduction onset potential in organic electrolyte (acetonitrile) was −0.21 V for **gNDI-T** and −0.02 V for **gNDI-V**. A shift in the onset of reduction towards more positive potentials for both copolymers was observed when switching from an organic electrolyte to aqueous electrolyte, and similar results have been reported for our previous NDI-based copolymers.[16] The reduction onset potential shift is attributed to changes in both the size and charge density of the counter cations and differences in the solute–solvent interactions between the polymer and the supporting electrolyte.[61] The highly hydrophilic OEG side chains were introduced to NDI copolymers, allowing for efficient ionic species transport in aqueous media.[62] Compared with acetonitrile, the stronger interactions between OEG side chains and water will lead to favorable K^+ penetration into the polymer film to stabilize the negative charge on the polymer backbone during reduction. Although **gNDI-V** (−4.40 eV) presents lower LUMO energy levels than **gNDI-T** (−4.21 eV), a more positive reduction onset potential in aqueous media was found in **gNDI-T** (0.13 V) than **gNDI-V** (0.06 V). According to the literature, the more positive reduction onset potential found in **gNDI-T** is due to its less ordered molecular packing, which is expected to facilitate ion penetration into the polymer bulk.[49,63,64]

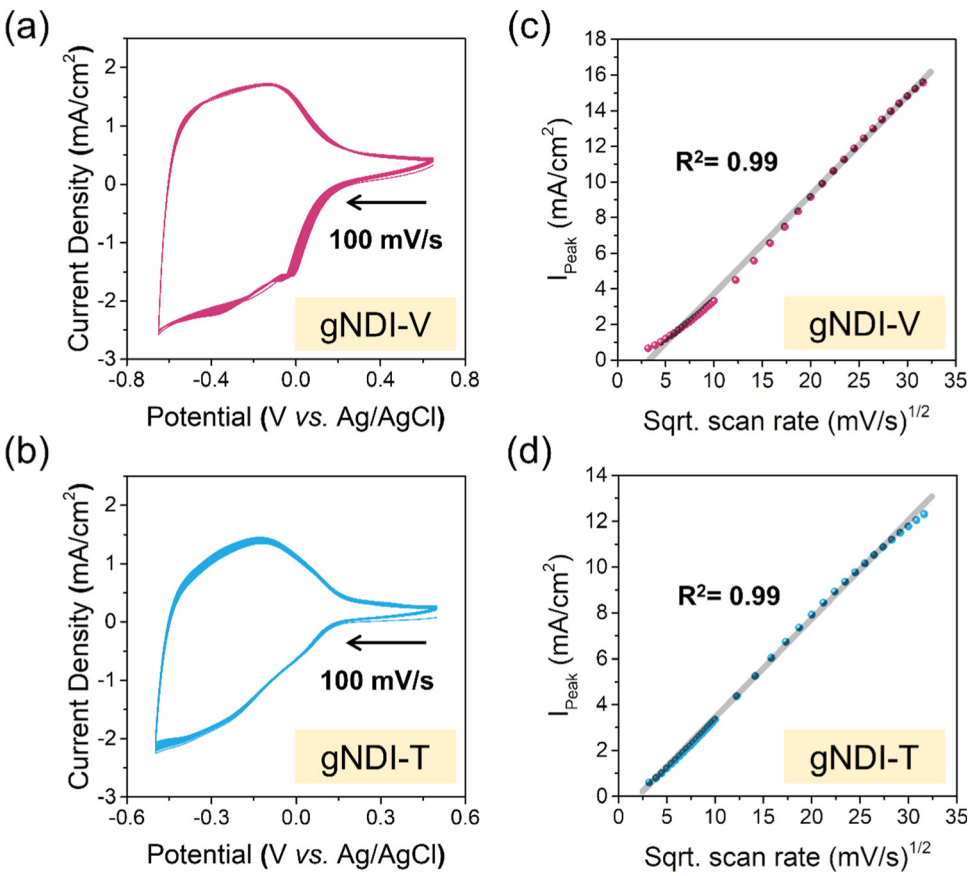

Fig. 4 Reversible charging of (a) **gNDI-V** (−0.65 V to 0.65 V) and (b) **gNDI-T** (−0.50 V to 0.50 V) with 0.1 M $KCl_{(aq)}$ electrolyte over 150 cycles at a scan rate of 100 mV s^{-1}. The arrows indicate scan directions. (c) **gNDI-V** and (d) **gNDI-T** were measured by CV measurements at different scan rates from 10 to 1000 mV s^{-1}, and the extracted peak current density in CVs is shown as a function of the square roots of scan rates.

To evaluate the electrochemical stability, the copolymer films were continuously charged for 150 cycles in Fig. 4a andb. As in previous discussions, the **gNDI-T** exhibits a more positive reduction onset potential which indicates **gNDI-T** would reach a higher doping level than **gNDI-V** during the same potential window (−0.65 V to 0.65 V). A lower charging stability was found for **gNDI-T** than **gNDI-V** during the same potential window (−0.65 V to 0.65 V) (Fig. S12, ESI†), which was likely due to its instability at a higher doping level.[16] Then, a narrower potential window (0.50 V to −0.50 V) was applied and the charging stability was significantly improved for **gNDI-T**. Notably, the larger charging window (−0.65 V to 0.65 V) found in **gNDI-V** results from its ordered molecular packing, which benefits from its coplanar backbone conformation. In addition to the electrochemical stability, the redox kinetics of polymer films in aqueous electrolyte was studied as well. CV measurements of copolymers in 0.1 M KCl aqueous solution from −0.65 V to 0.65 V for **gNDI-V** and from −0.50 V to 0.50 V for **gNDI-T** at a scan rate from 10 mV s^{-1} to 1000 mV s^{-1} were carried out (Fig. S13, ESI†). As shown in Fig. 4c and d, the linear trend of relationship between current intensity and square root of scan rate has been shown in both copolymers, which reveals a diffusion-controlled mechanism of oxidation/reduction reactions in accordance with the Randles–Sevcik equation.[65]

2.6 Electrochromic properties

To investigate the electrochemical doping mechanism of NDI-based copolymers in aqueous electrolyte, we conducted spectroelectrochemical measurements of the thin films and monitored their absorption spectra changes during the cycling in Fig. 5a. Similar absorption spectra changes for **gNDI-V** and **gNDI-T** were observed. Note that the evolution of a new absorption (620–900 nm) and loss in the intensity of the ICT band (450–650 nm) were observed within the voltage range from 0.1 V to −0.7 V *vs.* Ag/AgCl, indicating the formation of the polaron.[66] In addition, the polaron formation is also observed when a voltage pulse is applied as shown in Fig. S14 (ESI†), where the difference plots were obtained by subtracting the pristine absorption spectrum (0.1 V) from the electrochemically doped ones. A quantitative way to evaluate the electrochemical doping efficiency is shown in Fig. 5b, where the integral of the polaron absorption (620–900 nm) and the ICT absorption band (450–650 nm) were plotted *versus* the applied voltage.[67] From 0.1 V to −0.2 V, similar slopes in the polaron and ICT absorption band were found. However, from −0.2 V to −0.7 V, a higher slope was found in **gNDI-V** than **gNDI-T**, which indicates the higher magnitude of ionic–electronic coupling in **gNDI-V**.[67]

Furthermore, electrochromic behavior during spectroelectrochemical measurements was found for the two copolymers and the electrochromic behavior was studied in Fig. 5c and the corresponding data is summarized in Table S3 (ESI†). To study the kinetics of the electrochromic switching process, the films of NDI-based copolymers were investigated *via* chronoabsorptiometry on films spin cast onto ITO/glass. The transmittance of the thin films was monitored by applying sequential square wave bias pulses, which switched the film between 0.1 V and −0.7 V. **gNDI-V** exhibited a higher electrochromic contrast (ΔT = 30%) than **gNDI-T** (ΔT = 19%). Besides, a faster coloration (T_c, 0.4 s) and bleaching time (T_b, 0.4 s) of **gNDI-V** was found compared with **gNDI-T** (T_c, 1.5 s, T_b, 0.4 s). Moreover, both NDI-based copolymers showed good long-term switching stability with less than 2% drop in coloration contrast after switching

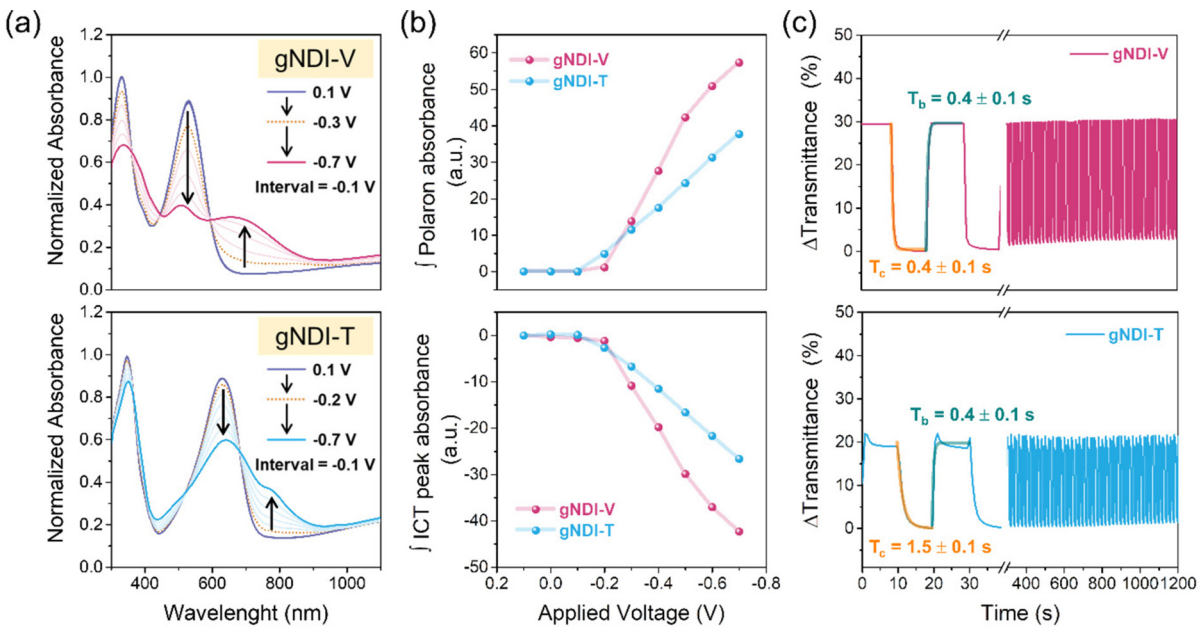

Fig. 5 (a) Spectroelectrochemical measurements of NDI copolymers, monitoring the evolution of the absorption spectra of polymer thin films between +0.1 V and −0.7 V *vs.* Ag/AgCl at a scan rate of 100 mV s^{-1}, voltage step of 0.1 V. (b) Integrals of the polaron absorption and the ICT absorption with the charging varied from 0.1 V to −0.7 V *vs.* Ag/AgCl in 0.1 M KCl aqueous solution. (c) Time-dependent transmittance changes during bleaching (−0.7 V) and coloration (0.1 V) of electrochromic properties based on **gNDI-V** and **gNDI-T**, recorded at 532 nm and 623 nm, respectively.

for 1200 s. In addition, since the ideal electrochromic material displays a large transmittance change with a small amount of charge, the composite coloration efficiency (CCE, η) was used to evaluate the power efficiency during the electrochromic switching process, and calculated as eqn (2)[68]

$$\eta = \frac{\Delta OD}{\Delta Q} = \frac{\log(T_{bl}/T_{co})}{\Delta Q} \quad (2)$$

where ΔOD is the change in optical density defined by the logarithm of the ratio between the transmittance at the bleached state (T_{bl}) and the colored state (T_{co}) and ΔQ presents the injected charge per unit area. Fig. S15 (ESI†) shows plots of ΔOD as a function of ΔQ for the electrochromic devices (ECDs) based on **gNDI-V** and **gNDI-T**, from which the η values were obtained from the linear slopes. The composite coloration efficiency of **gNDI-V** (1988 $cm^2\ C^{-1}$) was much higher than that of **gNDI-T** (391 $cm^2\ C^{-1}$), which was in accordance with the electrochemical doping efficiency found in spectroelectrochemical measurements. Specifically, the higher electrochemical doping efficiency and CCE were attributed to the higher magnitude of ionic–electronic coupling in **gNDI-V** thin film owing to the coplanar backbone conformation and favorable molecular packing which facilate ion–electron transport. Moreover, **gNDI-V** exhibited an impressive electrochromic performance compared with those state-of-the-art copolymer-based ECDs (Table S3, ESI†).

2.7 OECTs performance

To investigate the mixed ionic–electronic transport properties of NDI-based copolymers, **gNDI-V** and **gNDI-T** were studied as channel materials by fabricating OECTs. The key figure of merit, transconductance g_m, at saturation conditions for OECTs is obtained from eqn (3):[69]

$$g_m = \frac{Wd}{L}\mu C^*(V_{TH} - V_G) \quad (3)$$

where V_G is the gate voltage and V_{TH} is the threshold voltage; W presents the channel width, d and L are the channel depth and the channel length, respectively; μ is the charge-carrier mobility and C^* presents the volume capacitance. The value of μC^* is used for evaluating the ionic–electronic conduction properties of the channel materials. The detailed OECT parameters for both NDI-based copolymers were summarized in Table 2 and Table S4 (ESI†).

gNDI-V with more coplanar backbone conformation driven by intramolecular hydrogen bonding exhibited higher device performance than **gNDI-T**. **gNDI-V** reached a maximum drain current of 2.82 mA (V_G = 0.65 V), which is more than 4-fold higher than **gNDI-T** (0.62 mA, V_G = 0.50 V) at the same V_D = 0.4 V (see Fig. 6a and b). Note that the maximum drain current found for **gNDI-T** was at V_G = 0.50 V and V_D = 0.4 V. As for the normalized transconductance, $g_{m,norm}$ in Fig. 6c and d, **gNDI-V** also gives a higher value (0.42 S cm^{-1}) than **gNDI-T** (0.11 S cm^{-1}). Additionally, the window width of the hysteresis of **gNDI-V** (17 mV) is larger than **gNDI-T** (9 mV), indicating easier ion diffusion in **gNDI-T**.[70] As shown in Fig. S16 (ESI†), the threshold voltage (V_{TH}) is 0.30 V for **gNDI-V** and 0.20 V for **gNDI-T**, which is in accordance with the trend of the reduction onset observed from CV curves in aqueous media.

To systematically investigate the response time, the on/off-time constant (τ_{on}/τ_{off}) was provided in Fig. S17 (ESI†). Additionally, for the analyte-responsive sensor, their response times are usually recorded at 90% of the saturation values. The rise/fall ($T_{on,90\%}/T_{off,90\%}$) response times were obtained by measuring the time it takes for the channel current (I_{DS}) to reach 90% of its maximum and minimum value. To eliminate the thickness effects,[71] the response time was normalized by channel geometry ($\tau_{norm} = \tau/(d(WL)^{1/2})$ and $T_{norm,90\%} = T/(d(WL)^{1/2})$) according to the literature.[72] A normalized response time $\tau_{on,\ norm}/\tau_{off,\ norm}$ of 2.90/0.32 ms μm^{-2} ($T_{on,\ norm,90\%}/T_{off,norm,\ 90\%}$ of 7.61/0.65 ms μm^{-2}) and 0.87/0.18 ms μm^{-2} ($T_{on,norm,90\%}/T_{off,norm,90\%}$ of 2.33/0.42 ms μm^{-2}) was found for **gNDI-V** and **gNDI-T**, respectively. As discussed in the charging behavior section, the faster response time for **gNDI-T** is attributed to its less ordered packing, which facilitates ion penetration into the polymer bulk. Besides, the asymmetry in the switching characteristics between the turn-on and turn-off times was found, indicating the presence of a dissipation process, such as a viscoelastic component in the conducting pathway through the channel. As reported, the possible processes that affect the formation of this pathway are (1) the doping of the NDI-based chains that affect electron density n_e and (2) the relaxation of intrachain conformations and interchain packing that affects electron mobility μ_e.[73,74] In addition, the on-to-off current ratios measured are in the order of 10^4–10^5, which can be comparable with the reported n-type copolymers.

To understand the volumetric doping process of NDI-based copolymers, the electrochemical impedance spectroscopy (EIS) technique was used as presented in the Fig. S18 (ESI†).[75] The capacitance was extracted by fitting EIS data *via* an equivalent circuit model (R_s ($R_p \| C$)), where the electrolyte resistance is R_s, and R_p and C present the polymer film's resistance and film's capacitance, respectively.[76] **gNDI-V** exhibited a lower volumetric capacitance (144 F cm^{-3}) than the **gNDI-T** films (237 F cm^{-3}).

Table 2 OECTs key performance metrics

Polymer	$g_{m,norm}$[a] (S cm^{-1})	μC^*[b] (F V^{-1} cm^{-1} s^{-1})	C^*[c] (F cm^{-3})	$\mu_{e,est}$[d] (cm^2 V^{-1} s^{-1})
gNDI-V	0.42 ± 0.02	2.31	144 ± 5	$1.4 \times 10^{-2} \pm 1.3 \times 10^{-3}$
gNDI-T	0.11 ± 0.01	0.42	237 ± 8	$1.5 \times 10^{-3} \pm 2.0 \times 10^{-4}$

[a] Normalized by channel geometry. [b] Extracted from the slope in plots of g_m *versus* $(Wd/L)[V_{TH} - V_G]$. [c] Measured by the electrochemical impedance spectroscopy. [d] Obtained from the figure of merit (μC^*) and volumetric capacitance (C^*).

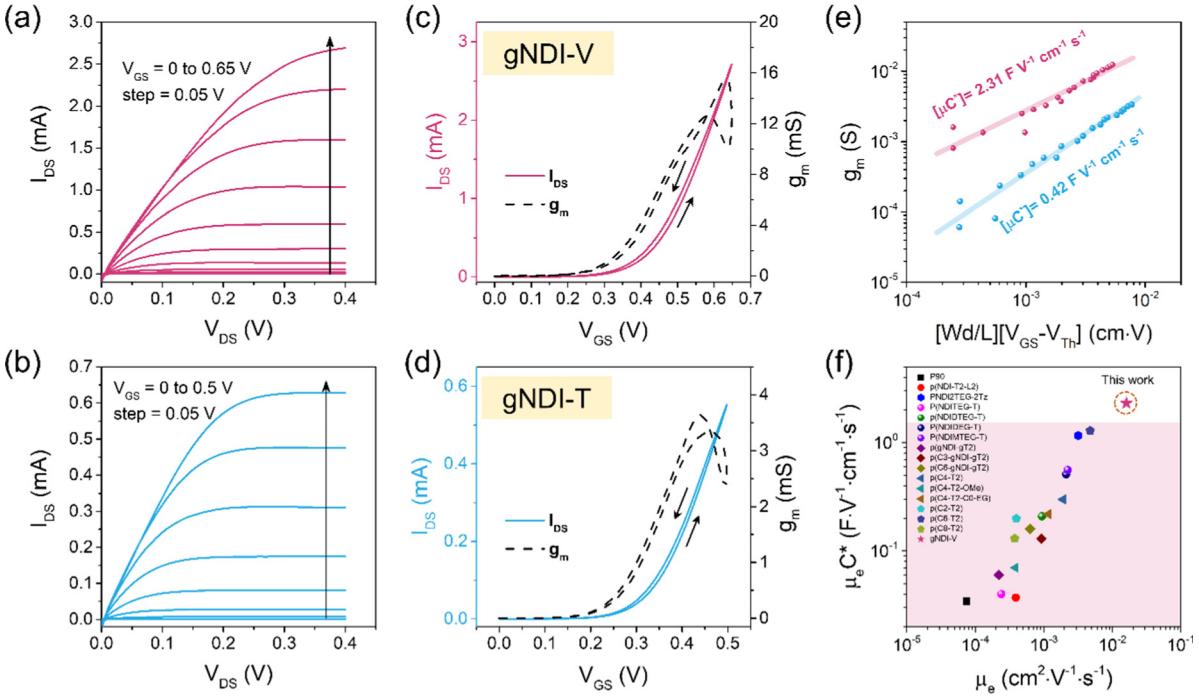

Fig. 6 (a and b) Output characteristics of OECTs based on gNDI-V and gNDI-T; (c and d) Transfer curve and transconductance g_m of the OECTs based on gNDI-V and gNDI-T. Devices were performed at a drain bias of V_{DS} = 0.4 V with a 0.1 M KCl aqueous electrolyte. (e) Plots of the transconductance against channel geometry and operation parameters to extract the associated μC^*. (f) The figure of merit μC^* for n-type NDI-based copolymers as a function of electron mobility (μ_e).

Similarly, the larger C^* is attributed to the less ordered packing of **gNDI-T**, which is expected to facilitate ion penetration into the polymer bulk. As shown in Fig. 6e, the μC^* increased more than five times going from 0.42 F V^{-1} cm^{-1} s^{-1} for **gNDI-T** to 2.31 F V^{-1} cm^{-1} s^{-1} for **gNDI-V**. Furthermore, based on the μC^* and C^* values, the electron mobility (μ) was obtained. Note that the two polymers both exhibited a good device reproducibility (see Fig. S19, ESI†). The average μ value (1.4×10^{-2} cm^2 V^{-1} s^{-1}) of **gNDI-V** is one order of magnitude higher than that (1.5×10^{-3} cm^2 V^{-1} s^{-1}) of **gNDI-T**, which benefits from the favorable molecular packing, originating from the coplanar backbone conformation driven by hydrogen bond functionalization. Note that the μC^* (2.31 F V^{-1} cm^{-1} s^{-1}) and μ (1.4×10^{-2} cm^2 V^{-1} s^{-1}) for **gNDI-V** are the highest values reported to date for the NDI-based OECTs (see Table S5, ESI†), which supports that our hydrogen bond functionalization opens up a proposing avenue for designing n-type mixed polymeric conductors operating in aqueous electrolyte. Long term on–off switching tests were performed to demonstrate the stable operation of NDI-based copolymers. The percentage retention of the initial current was employed to evaluate the operational stability. As summarized in Fig. S20 (ESI†), both NDI-based copolymers displayed a long-term stability with less than 9% current loss after 60 mins. According to the literature,[60] the aqueous stability is dependent on the film microstructural crystallinity and composition. Compared with the GIWAXS in the pristine and reduced state, it was found that the two NDI-based copolymers both retain good film microstructural crystallinity upon electrochemical doping, which accounts for the operational stability for the 60 minutes test.

3. Conclusion

In summary, high performance n-type polymeric mixed conductors have been designed and synthesized *via* manipulating the coplanar backbone conformation through intramolecular hydrogen bonds. We find that the coplanar backbone conformation driven by hydrogen bonding not only affects the copolymers' optical properties, electrochemical redox behavior and molecular packing, but also remarkably enhances the performance of aqueous-based electrochemical devices. **gNDI-V** exhibited a larger electrochromic contrast (ΔT = 30%) and a higher coloration efficiency (1988 cm^2 C^{-1}) than **gNDI-T**, which was due to its better ionic–electronic coupling. As for OECTs, **gNDI-V** outperformed **gNDI-T**, including a higher transconductance of 0.42 S cm^{-1} and exhibiting the highest value of μ (0.014 cm^2 V^{-1} s^{-1}) and μC^* (2.31 F V^{-1} cm^{-1} s^{-1}) for the NDI-based OECTs, which was attributed to the improved thin-film crystallinity and molecular packing induced by hydrogen bonding. This systematic work elucidates the mechanism of how hydrogen bonds promote the desired molecular conformation, solid-state packing, and electrochemical performances of n-type semiconducting polymeric materials. Moreover, we believe the hydrogen-bonding functionalization will provide rational design guidelines at **the** molecular level for researchers

from diverse backgrounds to develop high performance n-type polymeric materials operating in aqueous electrolyte.

Author contributions

J. Chen carried out most experiments and the data analysis; S. Cong designed and synthesized the polymers; L. Wang conducted the DFT calculations and analyzed the data with support from Y. Zhou; Y. Wang, L. Lan and Z. Li provided helpful discussions; C. Chen coordinated the work; I. McCulloch and W. Yue supervised the work; and J. Chen prepared the manuscript with support from all co-authors; all authors discussed the results and contributed to this work.

Conflicts of interest

There are no conflicts of interest to declare.

Acknowledgements

The authors thank the National Natural Science Foundation of China (Grant No. 21875291), the China Postdoctoral Foundation (Grant No. 2021M693580), and the GuangDong Basic and Applied Basic Research Foundation (Grant No. 2021A1515110261) for the financial support.

References

1 B. D. Paulsen, K. Tybrandt, E. Stavrinidou and J. Rivnay, *Nat. Mater.*, 2020, **19**, 13.
2 N. A. Kukhta, A. Marks and C. K. Luscombe, *Chem. Rev.*, 2022, **122**, 4325.
3 S. T. M. Tan, A. Gumyusenge, T. J. Quill, G. S. LeCroy, G. E. Bonacchini, I. Denti and A. Salleo, *Adv. Mater.*, 2022, **34**, 2110406.
4 J. Rivnay, S. Inal, B. A. Collins, M. Sessolo, E. Stavrinidou, X. Strakosas, C. Tassone, D. M. Delongchamp and G. G. Malliaras, *Nat. Commun.*, 2016, **7**, 11287.
5 C. Zhao, Z. Chen, R. Shi, X. Yang and T. Zhang, *Adv. Mater.*, 2020, **32**, e1907296.
6 Y. Wang, L. Feng and S. Wang, *Adv. Funct. Mater.*, 2019, **29**, 1806818.
7 E. Zeglio and O. Inganas, *Adv. Mater.*, 2018, **30**, 1800941.
8 Y. Dai, S. Dai, N. Li, Y. Li, M. Moser, J. Strzalka, A. Prominski, Y. Liu, Q. Zhang, S. Li, H. Hu, W. Liu, S. Chatterji, P. Cheng, B. Tian, I. McCulloch, J. Xu and S. Wang, *Adv. Mater.*, 2022, **34**, e2201178.
9 W. J. Song, S. Lee, G. Song, H. B. Son, D.-Y. Han, I. Jeong, Y. Bang and S. Park, *Energy Storage Mater.*, 2020, **30**, 260.
10 H. Zhang, X. Liu, H. Li, I. Hasa and S. Passerini, *Angew. Chem., Int. Ed.*, 2021, **60**, 598.
11 K. Schlingman, Y. Chen, R. S. Carmichael and T. B. Carmichael, *Adv. Mater.*, 2021, **33**, e2006863.
12 Y. Wang, E. Zeglio, L. Wang, S. Cong, G. Zhu, H. Liao, J. Duan, Y. Zhou, Z. Li, D. Mawad, A. Herland, W. Yue and I. McCulloch, *Adv. Funct. Mater.*, 2022, **32**, 2111439.
13 V. Rai, R. S. Singh, D. J. Blackwood and D. Zhili, *Adv. Eng. Mater.*, 2020, **22**, 2000082.
14 S. Cong, A. Creamer, Z. Fei, S. A. J. Hillman, C. Rapley, J. Nelson and M. Heeney, *Macromol. Biosci.*, 2020, **20**, 2000087.
15 L. R. MacFarlane, H. Shaikh, J. D. Garcia-Hernandez, M. Vespa, T. Fukui and I. Manners, *Nat. Rev. Mater.*, 2020, **6**, 7.
16 S. Cong, J. Chen, L. Wang, L. Lan, Y. Wang, H. Dai, H. Liao, Y. Zhou, Y. Yu, J. Duan, Z. Li, I. McCulloch and W. Yue, *Adv. Funct. Mater.*, 2022, **32**, 2201821.
17 B. Ding, G. Kim, Y. Kim, F. D. Eisner, E. Gutierrez-Fernandez, J. Martin, M. H. Yoon and M. Heeney, *Angew. Chem., Int. Ed.*, 2021, **60**, 19679.
18 X. Li, Y. Li, K. Sarang, J. Lutkenhaus and R. Verduzco, *Adv. Funct. Mater.*, 2021, **31**, 2009263.
19 T. J. Quill, G. LeCroy, A. Melianas, D. Rawlings, Q. Thiburce, R. Sheelamanthula, C. Cheng, Y. Tuchman, S. T. Keene, I. McCulloch, R. A. Segalman, M. L. Chabinyc and A. Salleo, *Adv. Funct. Mater.*, 2021, **31**, 2104301.
20 Z. S. Parr, R. B. Rashid, B. D. Paulsen, B. Poggi, E. Tan, M. Freeley, M. Palma, I. Abrahams, J. Rivnay and C. B. Nielsen, *Adv. Electron. Mater.*, 2020, **6**, 2000215.
21 Z. S. Parr, J. Borges-Gonzalez, R. B. Rashid, K. J. Thorley, D. Meli, B. D. Paulsen, J. Strzalka, J. Rivnay and C. B. Nielsen, *Adv. Mater.*, 2022, **34**, e2107829.
22 A. Savva, D. Ohayon, J. Surgailis, A. F. Paterson, T. C. Hidalgo, X. Chen, I. P. Maria, B. D. Paulsen, A. J. Petty, J. Rivnay, I. McCulloch and S. Inal, *Adv. Electron. Mater.*, 2019, **5**, 1900249.
23 H. Sun, M. Vagin, S. Wang, X. Crispin, R. Forchheimer, M. Berggren and S. Fabiano, *Adv. Mater.*, 2018, **30**, 1704916.
24 C. Y. Yang, D. Tu, T. P. Ruoko, J. Y. Gerasimov, H. Y. Wu, P. C. Harikesh, M. Massetti, M. A. Stoeckel, R. Kroon, C. Müller, M. Berggren and S. Fabiano, *Adv. Electron. Mater.*, 2021, **8**, 2100907.
25 C. Zhu, Z. Zhao, H. Chen, L. Zheng, X. Li, J. Chen, Y. Sun, F. Liu, Y. Guo and Y. Liu, *J. Am. Chem. Soc.*, 2017, **139**, 17735.
26 Y. Wang, T. Hasegawa, H. Matsumoto, T. Mori and T. Michinobu, *Adv. Mater.*, 2018, **30**, e1707164.
27 B. Sun, W. Hong, Z. Yan, H. Aziz and Y. Li, *Adv. Mater.*, 2014, **26**, 2636.
28 C. Zhu and L. Fang, *Macromol. Rapid Commun.*, 2018, **39**, 1700241.
29 C. Zhu, A. J. Kalin and L. Fang, *Acc. Chem. Res.*, 2019, **52**, 1089.
30 H. Huang, L. Yang, A. Facchetti and T. J. Marks, *Chem. Rev.*, 2017, **117**, 10291.
31 S. Wang, H. Li, K. Zhao, L. Zhang, Q. Zhang, X. Yu, H. Tian and Y. Han, *Macromolecules*, 2022, **55**, 2497.
32 T. Lei, X. Xia, J. Y. Wang, C. J. Liu and J. Pei, *J. Am. Chem. Soc.*, 2014, **136**, 2135.
33 Y. Zou, X. Ji, J. Cai, T. Yuan, D. J. Stanton, Y.-H. Lin, M. Naraghi and L. Fang, *Chem*, 2017, **2**, 139.
34 Q. Wang, S. Böckmann, F. Günther, M. Streiter, M. Zerson, A. D. Scaccabarozzi, W. L. Tan, H. Komber, C. Deibel,

R. Magerle, S. Gemming, C. R. McNeill, M. Caironi, M. R. Hansen and M. Sommer, *Chem. Mater.*, 2021, **33**, 2635.
35 Z. D. Yu, Y. Lu, J. Y. Wang and J. Pei, *Chem. Eur. J.*, 2020, **26**, 16194.
36 C. Zhu, A. U. Mu, Y. H. Lin, Z. H. Guo, T. Yuan, S. E. Wheeler and L. Fang, *Org. Lett.*, 2016, **18**, 6332.
37 D. Ohayon, A. Savva, W. Du, B. D. Paulsen, I. Uguz, R. S. Ashraf, J. Rivnay, I. McCulloch and S. Inal, *ACS Appl. Mater. Interfaces*, 2021, **13**, 4253.
38 I. P. Maria, B. D. Paulsen, A. Savva, D. Ohayon, R. Wu, R. Hallani, A. Basu, W. Du, T. D. Anthopoulos, S. Inal, J. Rivnay, I. McCulloch and A. Giovannitti, *Adv. Funct. Mater.*, 2021, **31**, 2008718.
39 J. Royakkers, K. Guo, D. T. W. Toolan, L. W. Feng, A. Minotto, D. G. Congrave, M. Danowska, W. Zeng, A. D. Bond, M. Al-Hashimi, T. J. Marks, A. Facchetti, F. Cacialli and H. Bronstein, *Angew. Chem., Int. Ed.*, 2021, **60**, 25005.
40 A. M. Evans, K. A. Collins, S. Xun, T. G. Allen, S. Jhulki, I. Castano, H. L. Smith, M. J. Strauss, A. K. Oanta, L. Liu, L. Sun, O. G. Reid, G. Sini, D. Puggioni, J. M. Rondinelli, T. Rajh, N. C. Gianneschi, A. Kahn, D. E. Freedman, H. Li, S. Barlow, G. Rumbles, J. L. Bredas, S. R. Marder and W. R. Dichtel, *Adv. Mater.*, 2022, **34**, e2101932.
41 A. Giovannitti, C. B. Nielsen, D. Sbircea, S. Inal, M. Donahue, M. R. Niazi, D. A. Hanifi, A. Amassian, G. G. Malliaras, J. Rivnay and I. McCulloch, *Nat. Commun.*, 2016, **7**, 13066.
42 D. Jeong, I. Y. Jo, S. Lee, J. H. Kim, Y. Kim, D. Kim, J. R. Reynolds, M. H. Yoon and B. J. Kim, *Adv. Funct. Mater.*, 2022, **32**, 2111950.
43 D. Rosas Villalva, S. Singh, L. A. Galuska, A. Sharma, J. Han, J. Liu, M. A. Haque, S. Jang, A. H. Emwas, L. J. A. Koster, X. Gu, B. C. Schroeder and D. Baran, *Mater. Horiz.*, 2022, **9**, 500.
44 H. Wei, Y. Liu, Z. Liu, J. Guo, P. A. Chen, X. Qiu, G. Dai, Y. Li, J. Yuan, L. Liao and Y. Hu, *Adv. Electron. Mater.*, 2020, **6**, 1901241.
45 S. Wang, D. Fazzi, Y. Puttisong, M. J. Jafari, Z. Chen, T. Ederth, J. W. Andreasen, W. M. Chen, A. Facchetti and S. Fabiano, *Chem. Mater.*, 2019, **31**, 3395.
46 B. D. Naab, X. Gu, T. Kurosawa, J. W. F. To, A. Salleo and Z. Bao, *Adv. Electron. Mater.*, 2016, **2**, 1600004.
47 M. Schubert, D. Dolfen, J. Frisch, S. Roland, R. Steyrleuthner, B. Stiller, Z. Chen, U. Scherf, N. Koch, A. Facchetti and D. Neher, *Adv. Energy Mater.*, 2012, **2**, 369.
48 L. Lan, J. Chen, Y. Wang, P. Li, Y. Yu, G. Zhu, Z. Li, T. Lei, W. Yue and I. McCulloch, *Chem. Mater.*, 2022, **34**, 1666.
49 K. Feng, W. Shan, S. Ma, Z. Wu, J. Chen, H. Guo, B. Liu, J. Wang, B. Li, H. Y. Woo, S. Fabiano, W. Huang and X. Guo, *Angew. Chem., Int. Ed.*, 2021, **60**, 24198.
50 X. Chen, A. Marks, B. D. Paulsen, R. Wu, R. B. Rashid, H. Chen, M. Alsufyani, J. Rivnay and I. McCulloch, *Angew. Chem., Int. Ed.*, 2021, **60**, 9368.
51 B. D. Paulsen, S. Fabiano and J. Rivnay, *Annu. Rev. Mater. Res.*, 2021, **51**, 73.
52 P. M. Alvey, R. J. Ono, C. W. Bielawski and B. L. Iverson, *Macromolecules*, 2013, **46**, 718.
53 S. Lee, G. S. Lee, M. Kang, Y. H. Ha, Y. H. Kim and D. S. Chung, *Adv. Funct. Mater.*, 2022, **32**, 2204383.
54 Y. Kim, J. Hong, J. H. Oh and C. Yang, *Chem. Mater.*, 2013, **25**, 3251.
55 Y. Wang, T. Hasegawa, H. Matsumoto and T. Michinobu, *J. Am. Chem. Soc.*, 2019, **141**, 3566.
56 J. H. Dou, Y. Q. Zheng, Z. F. Yao, Z. A. Yu, T. Lei, X. Shen, X. Y. Luo, J. Sun, S. D. Zhang, Y. F. Ding, G. Han, Y. Yi, J. Y. Wang and J. Pei, *J. Am. Chem. Soc.*, 2015, **137**, 15947.
57 M. H. Lee, J. Kim, M. Kang, J. Kim, B. Kang, H. Hwang, K. Cho and D. Y. Kim, *ACS Appl. Mater. Interfaces*, 2017, **9**, 2758.
58 A. Luzio, J. Martin, C. H. Cheng, N. Stingelin, M. F. Toney, A. Salleo and M. Caironi, *J. Mater. Chem. C*, 2021, **9**, 15848.
59 I. E. Jacobs, G. D'Avino, V. Lemaur, Y. Lin, Y. Huang, C. Chen, T. F. Harrelson, W. Wood, L. J. Spalek, T. Mustafa, C. A. O'Keefe, X. Ren, D. Simatos, D. Tjhe, M. Statz, J. W. Strzalka, J. K. Lee, I. McCulloch, S. Fratini, D. Beljonne and H. Sirringhaus, *J. Am. Chem. Soc.*, 2022, **144**, 3005.
60 S. M. Kim, C. H. Kim, Y. Kim, N. Kim, W. J. Lee, E. H. Lee, D. Kim, S. Park, K. Lee, J. Rivnay and M. H. Yoon, *Nat. Commun.*, 2018, **9**, 3858.
61 M. Moser, A. Savva, K. Thorley, B. D. Paulsen, T. C. Hidalgo, D. Ohayon, H. Chen, A. Giovannitti, A. Marks, N. Gasparini, A. Wadsworth, J. Rivnay, S. Inal and I. McCulloch, *Angew. Chem., Int. Ed.*, 2021, **60**, 7777.
62 A. Khot and B. M. Savoie, *J. Polym. Sci.*, 2022, **60**, 610.
63 L. Q. Flagg, C. G. Bischak, J. W. Onorato, R. B. Rashid, C. K. Luscombe and D. S. Ginger, *J. Am. Chem. Soc.*, 2019, **141**, 4345.
64 H. Jia, Z. Huang, P. Li, S. Zhang, Y. Wang, J.-Y. Wang, X. Gu and T. Lei, *J. Mater. Chem. C*, 2021, **9**, 4927.
65 M. Krajewski, B. Hamankiewicz, M. Michalska, M. Andrzejczuk, L. Lipinska and A. Czerwinski, *RSC Adv.*, 2017, **7**, 52151.
66 A. A. Szumska, I. P. Maria, L. Q. Flagg, A. Savva, J. Surgailis, B. D. Paulsen, D. Moia, X. Chen, S. Griggs, J. T. Mefford, R. B. Rashid, A. Marks, S. Inal, D. S. Ginger, A. Giovannitti and J. Nelson, *J. Am. Chem. Soc.*, 2021, **143**, 14795.
67 G. Krauss, F. Meichsner, A. Hochgesang, J. Mohanraj, S. Salehi, P. Schmode and M. Thelakkat, *Adv. Funct. Mater.*, 2021, **31**, 2010048.
68 Y. R. In, J. M. Han, J. E. Kwon, B.-G. Kim and H. C. Moon, *Chem. Eng. J.*, 2022, **433**, 13380.
69 J. Duan, G. Zhu, L. Wang, J. Chen, S. Cong, X. Zhu, Y. Zhou, Z. Li, I. McCulloch and W. Yue, *Adv. Funct. Mater.*, 2022, **32**, 2203937.
70 Y. Zhang, G. Ye, T. P. A. van der Pol, J. Dong, E. R. W. van Doremaele, I. Krauhausen, Y. Liu, P. Gkoupidenis, G. Portale, J. Song, R. C. Chiechi and Y. van de Burgt, *Adv. Funct. Mater.*, 2022, **32**, 2201593.
71 J. Rivnay, P. Leleux, M. Ferro, M. Sessolo, A. Williamson, D. A. Koutsouras, D. Khodagholy, M. Ramuz, X. Strakosas, R. M. Owens, C. Benar, J. Badier, C. Bernard and G. G. Malliaras, *Sci. Adv.*, 2015, **1**, e1400251.

72 X. Wu, M. Stephen, T. C. Hidalgo, T. Salim, J. Surgailis, A. Surendran, X. Su, T. Li, S. Inal and W. L. Leong, *Adv. Funct. Mater.*, 2022, **32**, 2108510.
73 J. T. Friedlein, M. J. Donahue, S. E. Shaheen, G. G. Malliaras and R. R. McLeod, *Adv. Mater.*, 2016, **28**, 8398.
74 A. Giovannitti, D. T. Sbircea, S. Inal, C. B. Nielsen, E. Bandiello, D. A. Hanifi, M. Sessolo, G. G. Malliaras, I. McCulloch and J. Rivnay, *Proc. Natl. Acad. Sci.*, 2016, **113**, 12017.
75 I. Del Agua, L. Porcarelli, V. F. Curto, A. Sanchez-Sanchez, E. Ismailova, G. G. Malliaras and D. Mecerreyes, *J. Mater. Chem. B*, 2018, **6**, 2901.
76 Y. Wang, A. Hamidi-Sakr, J. Surgailis, Y. Zhou, H. Liao, J. Chen, G. Zhu, Z. Li, S. Inal and W. Yue, *J. Mater. Chem. C*, 2021, **9**, 13338.

